Resonance Light Scattering in Dye-Aggregates Forming in Dewetting Droplets

Jean-Nicolas Tisserant,[†,‡] Rolf Brönnimann,[§] Roland Hany,[†] Sandra Jenatsch,[†,⊥] Frank A. Nüesch,[†,⊥] Raffaele Mezzenga,[‡] Gian-Luca Bona,[∥,#,▽] and Jakob Heier*[,†]

[†]Laboratory for Functional Polymers, Empa, Swiss Federal Laboratories for Materials Science and Technology, Überlandstrasse 129, CH-8600 Dübendorf, Switzerland, [‡]Food and Soft Materials Science, Institute of Food, Nutrition and Health, ETH Zürich, CH-8092 Zürich, Switzerland, [§]Laboratory for Electronics, Metrology and Reliability, Empa, Swiss Federal Laboratories for Materials Science and Technology, Überlandstrasse 129, CH-8600 Dübendorf, Switzerland, [⊥]Institut des Matériaux, Ecole Polytechnique Fédérale de Lausanne, EPFL Station 12, CH-1015 Lausanne, Switzerland, [∥]Empa, Swiss Federal Laboratories for Materials Science and Technology, Überlandstrasse 129, CH-8600 Dübendorf, Switzerland, [#]Department of Information Technology and Electrical Engineering, ETH Zürich, CH-8092 Zürich, Switzerland, and [▽]Laboratory for Photonic Materials and Characterization, École Polytechnique Fédérale de Lausanne (EPFL), CH-1015 Lausanne, Switzerland

ABSTRACT Small organic semiconducting molecules assembling into supramolecular J- and H- aggregates have attracted much attention due to outstanding optoelectronic properties. However, their easy and reproducible fabrication is not yet sufficiently developed for industrial applications, except for silver halide photography. Here we present a method based on aggregate precipitation during the phase separation and dewetting of the evaporating dye precursor solution. The smaller the precursor droplets, the more pronounced the J-aggregation. The aggregates cause the films to resonantly scatter incoming light. Because the dye aggregate extinction resonances have narrowest bandwidths, a wavelength selectivity is observed that exceeds the selectivity of localized surface plasmon resonances. The aggregation mechanism can be easily applied to periodically structured substrates, making the method appealing for photonic applications. We demonstrate this point with a 2D grating, where the narrow absorption range of the aggregates leads to wavelength specific (one color only) scattering.

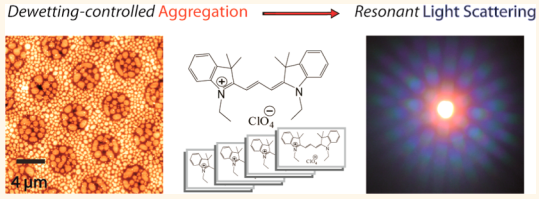

KEYWORDS: cyanine dye · J-aggregates · PCBM · absorption grating · photonic crystal · dewetting · resonant light scattering

In dye aggregates, the crystal-like supramolecular assembly of the molecules delocalizes the photoexcited state, forming large-scale coherently coupled molecular dipoles.[1−3] The stacking accounts for specific optoelectronic properties, such as a narrow excitonic absorption band, superradiant emission, high nonlinear susceptibilities, efficient energy migration and superquenching.[4−6] Depending on the exact arrangement of the dye in the aggregate, either red-shifted J-aggregates or blue-shifted H-aggregates are observed. A large number of novel nanophotonic systems can be envisioned using the properties of aggregates, ranging from sensors,[7] nonlinear optical devices,[8] optical data recording,[9] photoelectron storage[10] to cavity quantum electrodynamic devices.[11] Aggregates also find useful applications in photonic crystals where a resonantly absorbing medium can create novel physical effects.[12]

Aggregates forming in solution and films are normally well characterized by their absorption characteristics. In aggregates with large volume and chromophores with strong electronic coupling, also Rayleigh scattering near the absorption band (Resonance light scattering, RLS) contributes to extinction.[13,14] An entire branch of biochemical and pharmaceutical analysis has been established based on enhanced RLS signals from aggregated chromophores on biomolecule templates.[15] To the best of our knowledge, no prior literature reports on deliberately manufactured dye films with enhanced resonance light scattering properties for use in devices. Differently, in materials with localized surface plasmon resonance (LSPR), numerous applications in nanoscale optics and photonics have been suggested because the huge scattering cross-section of such structures allows the detection of very small signals which

* Address correspondence to Jakob.heier@empa.ch.

Received for review May 16, 2014 and accepted September 9, 2014.

Published online September 09, 2014
10.1021/nn5040839

can be applied in nanoantennas and resonators. Other examples include solar cells to enhance the optical path length of light.[16,17]

Until now the only industrial application of cyanine J-aggregates is as spectral sensitizers in silver halide photography,[18] where the ability of cyanine dyes to adsorb at silver halide interfaces is exploited. Problematic for applications in optoelectronic devices is the reproducible immobilization of cyanine J-aggregates on different types of substrates.[19] Several techniques are investigated, including Langmuir–Blodgett films,[20] layer-by-layer deposition[21] and thin layer crystallization,[22] or as discovered more recently on dendrimer surface.[23] Of interest are methods utilizing a structuring matrix such as polymers[24] or nanocapsules.[25] We showed in earlier studies that spin coated blends of [6,6]-phenyl-C_{61}-butyric acid methyl ester (PCBM) and the cyanine dye 1,1′-diethyl-3,3,3′,3′-tetramethylcarbocyanine perchlorate (CyC) phase separate into a variety of morphologies.[26] For blend morphologies that develop dye domains smaller than some hundred nanometers, the dye organizes into H-aggregates. It is believed that confinement of supersaturated solutions in cavities formed between PCBM clusters induces the nucleation of H-aggregates which can relax into J-aggregates.[27,28]

More generally, the complex processes at solid–liquid interfaces or solid–liquid–air contact lines are considered to be of great interest in nanosciences as they are important for self-assembly.[29] The physics behind drying droplets is complex and involves evaporative convection, diffusion of solutes, Marangoni flows, wetting, dewetting, contact-line pinning, supersaturation and crystallization.[30] Evaporation at the contact line is strongly enhanced as discussed in numerous theoretical and experimental studies on millimeter sized droplets.[31,32] A few studies demonstrate nanoparticle assembly from evaporating micron sized droplets.[33] Bao exploited that mechanism for the droplet-pinned crystallization method.[34] These observations of rim nucleation in dye droplets also relate to our earlier work where we demonstrated the growth of large cyanine single crystals from nuclei forming in dewetted dye droplets.[35]

We show here that these principles can also be utilized to organize dye molecules either into J- or H-aggregates. The process is universal, and we demonstrate it for dye films dewetting from different substrates and for a blend system that phase separates by liquid–liquid dewetting. Characteristic to dye molecules assembled by these processes is that they scatter light resonantly, independent of the exact manufacturing procedure or the type of aggregate.

RESULTS AND DISCUSSION

Cyanine Aggregate Formation in Dewetting Films. In a first experiment we manufacture dye droplets by a dewetting process.[36,37] Cyanine films dewet from glass substrates when spin coated from saturated ethanol solutions forming micrometer-sized domains (Figure 1a). The UV–vis spectrum of the film shows monomer absorption (580 nm), dimer absorption (525 nm), and a weak shoulder at 480 nm associated with H-aggregation. This spectrum does not differ from the absorbance spectrum of a uniform dye film. Following the arguments from above, a bigger ratio of perimeter to volume should enhance aggregation. A strategy to reduce the droplet size is to deposit the solution onto nanostructured substrates where the droplets are contact-line pinned to the surface. The mechanism of dewetting on heterogeneous surfaces has been studied both theoretically[38] and experimentally.[39] It allows to tune the size and distribution of the dewetted droplets *via* the characteristics of the surface heterogeneities.

Nanostructured substrates were manufactured from organic phase separating blend films by selectively removing one of the two components from the film. The dimensions of the nanostructures are then determined by the characteristic wavelength of the phase separating system. Here we used PCBM and PCB–diyne (for structure see Supporting Information Figure 1) nanostructures resulting from PCBM/CyC[26] and PCB–diyne/CyC[40] phase separation and polystyrene (PS) nanostructures resulting from phase separation with poly(vinyl methyl ether) PVME.[41] Alternatively, gold substrates have been patterned by self-assembled monolayers (SAMs).[42] The substrates were subsequently coated with a saturated solution of dye. Scanning probe microscope (SPM) images of nanostructured substrates and the corresponding dewetted CyC films are shown in the Supporting Information Figure 2. On all substrates, the dye forms a dense array of individual domains that show an almost monodisperse size distribution in the submicrometer range. As a general trend it can be observed that the smaller the substrate features, the smaller the dewetting domains. SPM images of dewetted CyC films and the associated UV–vis spectra on such substrates are shown in Figure 1b–f.

In the UV–vis spectra, next to monomer (M) and dimer (D) absorption, in all dye films, a red-shifted peak at 593 nm (J-aggregate) and a weak shoulder at 480 nm characteristic for H-aggregation are visible. The spectra show features in nonabsorbing regions of the sample (long wavelength tail), these features as well as significant fractions of the aggregate peaks arise from resonance light scattering (RLS). This type of scattering is rather unconventional and will be discussed later in full detail.

In films deposited from isopropyl alcohol solutions onto gold substrates that have been patterned by self-assembled monolayers (SAMs) the films fully dewet from the octadecanethiol SAM, but show small

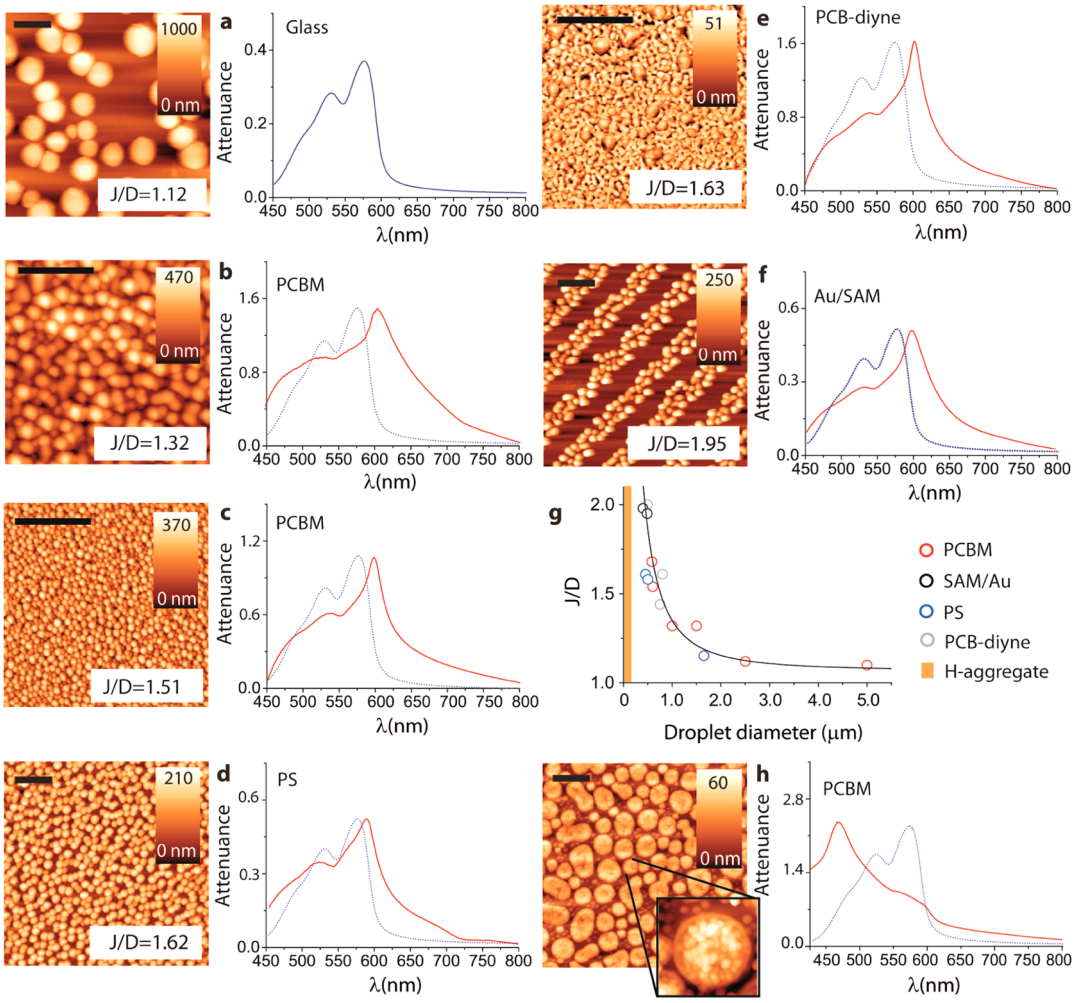

Figure 1. Morphology and UV−vis spectra of dewetting droplets of CyC on different structured surfaces. CyC was coated from saturated ethanol solutions at 1000 rpm, (a) on glass and (b and c) on nanostructured PCBM surfaces. (d) CyC dewetting droplets on a nanostructured PS substrate, (e) on a PCB−diyne surface, and (f) on patterned self-assembled monolayers (SAMs), CyC coated from isopropyl alcohol. In all samples, the attenuance peaks contain a contribution of a scattering component. (g) J-aggregation trend (J/D) as a function of the droplet diameter for all templates. (h) CyC recoated on a nanostructured PCBM surface with large-scale (micrometer range) dewetting features. The inset shows that these PCBM domains are composed of subdomains. H-aggregates crystallize inside the cavities of the nanoporous PCBM. The size of the scale bars is 3.2 μm.

dewetting features on the gold stripes (Figure 1f). This is an important observation as it generalizes the types of surfaces on which dewetting can be controlled. We will demonstrate this in a later section by applying the mechanism to a simple Bragg grating.

As the dimer peak can be identified in all samples, we define the ratio of the peak attenuance at the J-aggregate position to the peak attenuance of the dimer (J/D) as a measure for the quality of a J-aggregate. A plot of (J/D) as a function of the dewetting droplet diameter for different substrates is shown in Figure 1g. All data collapse onto one master curve that shows an r^{-2} dependence, as indicated by the solid line (guide to the eye only), suggesting that the process indeed only depends on the droplet diameter, but not on the underlying substrate. An r^{-2} dependence is expected when aggregation occurs only at the droplet-substrate contact line and the phenomenon critically depends on the ratio of the volume of a droplet to the circumference of that droplet. Similarly to the "coffee stain effect" described by Deegan,[31] we believe that increased solvent evaporation at the pinned contact line of the droplets induces a capillary flow from the center to the rim where the dye aggregates.

The trend in Figure 1g suggests that decreasing the size of the dewetting droplets further should also result in more prominent J-aggregates. This proved difficult due to the surface tension of the droplets and could not be achieved even by using substrates with smaller topographical surface features. The volume of the dye droplets could be decreased only by confining the solution within a nanoporous substrate film. The inset in Figure 1h shows a structured PCBM film composed of nanoporous domains. In this case, the dye solution does not dewet from the substrate but is partially readsorbed in the PCBM cavities. We here also

observed aggregation, but the dye molecules organize such that now H-aggregates are formed (Figure 1h). The formation of H-aggregates in dye volumes confined by a PCBM matrix was investigated by us earlier.[43] Not only do the H-aggregates form spontaneously during spin-coating of dye solutions onto a nanoporous PCBM film as observed here, but the same type of H-aggregate also formed in PCBM/dye blend films, where the PCBM-phase established a similar nanostructure during coating.[28] The most relevant parameter is the size of the PCBM domains that determine the volume of the dye cavities. The PCBM substrates had been characterized by Mie-scattering, and H-aggregates were most pronounced in films with PCBM droplets of around 180 nm in diameter; the dye was thus confined in much smaller volumes than in dewetting droplets.

Cyanine Aggregate Formation in Blends. A direct proof of how closely related the formation processes for J- and H-aggregates are is given in blend films of the cyanine dye CyC and a fullerene derivate carrying one single long alkyl chain bearing a rigid diacetylene moiety (PCB−diyne). Here dewetting and phase separation compete, resulting in larger dye domains dewetting from the substrate and smaller dye domains confined in a PCB−diyne matrix (Figure 2a).[40] Experiments in which either PCB−diyne or the dye were selectively dissolved from the sample (Figure 2b,c) support the morphology sketched in Figure 2d. CyC forms large isolated domains and a surface layer of small domains on top of a PCB−diyne matrix. As concluded from the dewetting films and the cavity forming films, the J-aggregates form at the droplet−substrate contact line, while the H-aggregates form in the "bulk" of the small droplet.

The UV−vis spectra of these films are presented in Figure 2e. Additionally to the J-aggregation peak and a scattering tail, these samples show a broad shoulder around 480 nm indicative for H-aggregation. When the PCB−diyne phase is selectively dissolved in hexane, UV−vis spectra can give further insight in the location of the aggregates. Figure 2e shows that during this process dye in the form of dimers and H-aggregates disappeared to a large portion from the sample, leaving a film where most dye molecules are assembled as J-aggregates. In the Supporting Information Figure 3, the same UV−vis data after subtracting the PCBM signal is shown, proving that the changes in the H-aggregate signal are not due to the decreased PCBM background. The data prove that the H-aggregates are located in the small surface dye domains which are lifted off with PCB−diyne removal in hexane. The J-aggregates form in larger dye domains which are not affected by hexane. It can be argued that a herringbone structure would lead to two spectral features, the lower Davydov component (J-like) and the upper Davydov component (H-like) as observed for the

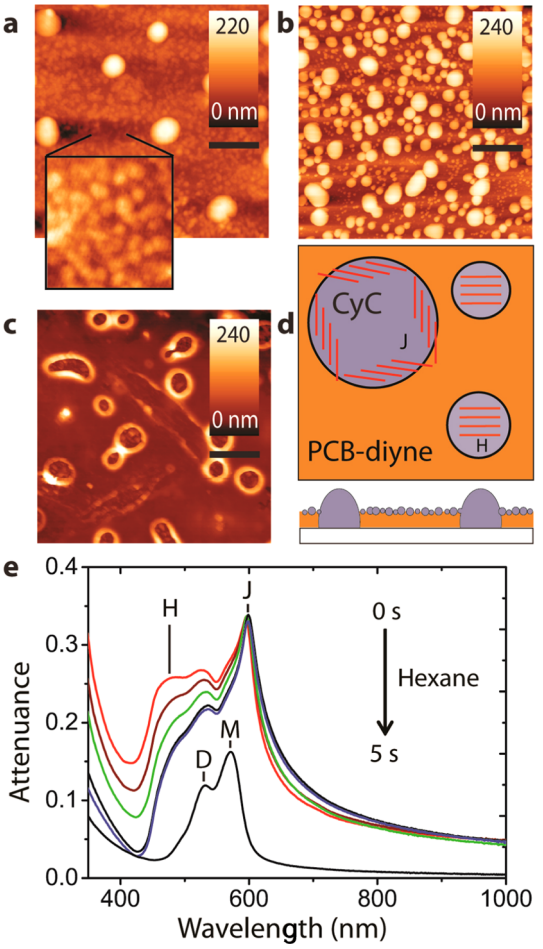

Figure 2. Aggregation in blends of PCB−diyne and CyC with a molar ratio of 2:1. (a) SPM image of a PCB−diyne/CyC blend film. SPM zoom showing the CyC nanodroplet phase. (b) SPM image after removing PCB−diyne in hexane, (c) after removing CyC in tetrafluoropropanol. The size of the scale bars is 3.2 μm. (d) Sketch of the phase morphology of spin-coated films. (e) UV−vis spectra showing H- and J-aggregates and monomer (M) and dimer (D) absorption of an amorphous film (raw data). The sample was dipped in hexane for approximately 1 s and a UV−vis spectrum was recorded. This procedure was repeated five times. The H-aggregate (H) shoulder decreases. Hexane dissolves PCB−diyne and lifts the small H-aggregate containing dye droplets off the sample.

CyC/PCB−diyne blend films. However, we prove by SPM that small cyanine domains containing H-aggregates only can be selectively removed from the sample, suggesting the coexistence of two independent aggregates. Furthermore, a herringbone structure should show fluorescence from the J-aggregate when excited in the H-aggregate. Experimentally, exciting CyC/PCB−diyne films at a wavelength around the H-aggregate peak did not show any fluorescence, while excitation in the J-band showed fluorescence.

To summarize, aggregates develop when the dye solution destabilizes into droplets during solvent evaporation and film formation. The droplets can either form during dewetting from a nanostructured surface or during phase separation (liquid−liquid dewetting)

from a blend solution. Aggregation was never observed when the solvent is evaporating from a uniform film; aggregation also only occurs in droplets with a diameter below a critical value. The literature suggests that H-aggregate formation is a bulk process, while J-aggregation is an interface phenomenon.[27] This is supported by our data. In confined domains, H-aggregates form independently of the nature of the interface since the dye droplet is in contact with a liquid phase during liquid−liquid dewetting or with a solid phase during dewetting.[28] J-aggregates, on the other hand, develop when the droplet evaporates from a solid surface. The strong domain radius dependence of J-aggregation links that process directly to the pinned contact line between air, substrate and solution of the evaporating droplet. We can only speculate why below a critical radius only H-aggregates form, here bulk and contact line region may merge and allow the formation of critical nuclei already in the bulk.

The two different experiments that demonstrate J-aggregation from dye droplets were conducted with solvents that are rather different in nature. Blend films were formed from chlorobenzene solutions; the choice was restricted to a common solvent for the dye and the fullerenes. Aggregates in dewetting films were formed from ethanol and isopropyl alcohol solutions not dissolving the underlying substrate structure. It is most surprising that aggregation is observed in different solvents as the flow conditions in evaporating droplets leading to nanoscale assembly are believed to depend strongly on solvent properties.[32] We attribute the difference in domain size for which J-aggregation occurs to the solvent. While in domains with a radius of 1.5 μm spin coated from ethanol almost no aggregation is visible (Figure 1), similar domains spin coated from chlorobenzene show a distinct aggregation peak (Figure 2). Still, it demonstrates the robustness of the process. Properties of solvents are summarized in the Supporting Information Table 1 and are an indication for the parameter window for aggregation.

Optical Properties of H- and J-Aggregates. Generally, transmission loss in forward direction (as measured by UV−vis) is not attributed to absorbance alone, but also scattering and reflection contribute to attenuance.[13] To quantify the fraction of light that contributes to scattering, the attenuance measured in UV−vis was compared to the absorption measured in an Ulbricht sphere[44] in aggregates of highest quality made from PCBM/CyC blends. In attenuance, the H-aggregate and J-aggregate samples show a sharp peak at 459 nm (2.70 eV) and 602 nm (2.06 eV), respectively. Nonaggregated films show a monomer peak at 580 nm (2.14 eV) and a dimer peak at 533 nm (2.33 eV) as well as an H-aggregate shoulder. In the integrating sphere, the sharp aggregate peaks vanish (Figure 3a). The overall absorption of the films can be fitted with Gaussians, assuming inhomogeneous broadening. For all film samples, we identify monomer and dimer absorption bands and a significant contribution in absorbance by H-aggregates. The J-aggregate absorption spectrum can only be fitted when we introduce a J-aggregate absorption peak at 587 nm (2.11 eV). The scattering efficiencies of the H- and J-aggregated dye are enormous, outnumbering the contribution of absorption. The scattering peak for H- and J-aggregate is blue and red-shifted, respectively, with respect to the absorption peaks. Both, the large share in scattering and the peak shift, can be attributed to the size of the aggregates. While the absorbance depends linearly on the aggregate volume, scattering shows a square dependence on aggregate volume.[13] Larger aggregates also show larger shifts with respect to monomer absorption.

Light at the aggregate absorption wavelength is scattered into a circle around the direction of light propagation (insets Figure 3b). The scattering pattern is a direct consequence of the droplet morphology of the films. A Fourier transformation of the droplet pattern shows a similar ring pattern (Supporting Information Figure 4). This result can be quantified by measuring the scattered light intensity as a function of wavelength and scattering angle. Figure 3b shows such 3D plots for J- and H-aggregates and an amorphous droplet film, significant scattering is only observed at the resonance wavelength of the aggregates. In nonaggregated dye films, attenuance (UV−vis) is somewhat higher than absorbance (Ulbricht sphere) representing reflected light; no significant scattering is noticeable.

The emission of J-aggregates is characterized by small Stokes-shifts and shortened fluorescence lifetime, but given the weak absorbance, we do not expect significant fluorescence from our samples. Indeed, emission spectra from different J-aggregate samples look alike and are superimposed with a large background signal. Compared to the monomer sample, the J-aggregate samples do not show a shoulder toward longer wavelengths (Supporting Information Figure 5).

Photonic Crystals. The specific scattering characteristics of J- and H-aggregates are exploited to add wavelength-selectivity to a Bragg grating. In a first step the wavelength dependent diffraction efficiency of an absorption grating composed of stripes of the nonaggregated dye is investigated. The grating has been manufactured by micromolding in capillaries[45] with a PDMS stamp with a channel periodicity of 2 μm and a diluted dye solution, resulting in a 120 nm thick topographical, but defect-rich grating. The attenuance spectrum resembles the true absorbance spectrum of the dye, a small scattering tail extends toward longer wavelengths. As a measure for the diffraction efficiency of the grating, the intensities of the first order diffraction peak are plotted (Figure 4a), see Materials and Methods. A notable dependence of the diffraction

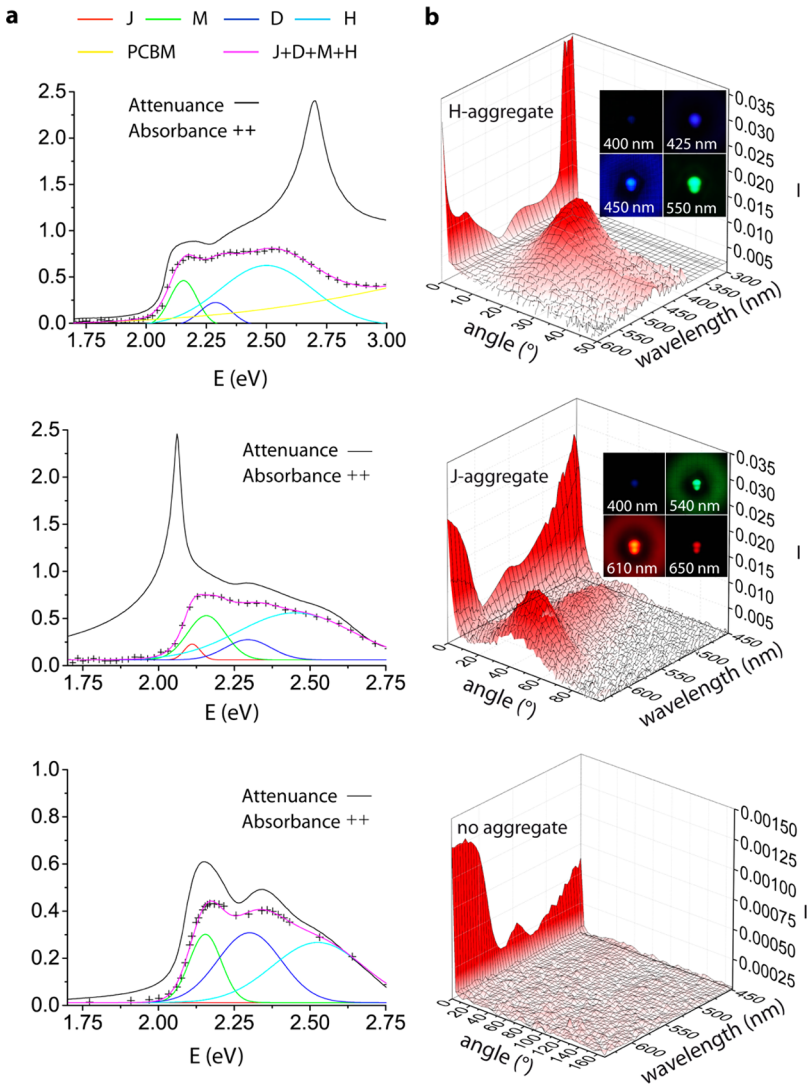

Figure 3. Resonance light scattering of aggregated films. (a) Attenuance spectra (UV−vis) and absorption spectra (Ulbricht sphere) of cyanine dye films containing H- and J-aggregates. The dye absorption spectra were fitted with four Gaussians accounting for monomer absorption at 2.14 eV, dimer absorption at 2.33 eV, H-aggregate and J-aggregate absorption. The integral of the J-aggregate curve is zero for the nonaggregated and H-aggregated films. PCBM absorption is subtracted where applicable. (b) Scattering intensity as a function of wavelength and scattering angle. The spectrum at an angle of 0° corresponds to the transmission spectrum. At the resonance wavelength, light is scattered into a defined solid angle determined by the topography of the films. No scattering is observed for nonaggregated samples. The *z*-scale at 0° angle has been arbitrarily rescaled such that absorbance and scattering features are visible on the same *z*-axis. The insets show photographs of monochromatic light scattered in forward direction.

efficiency on wavelength is found, with the efficiency peaking slightly red-shifted from the absorption maximum. A grating can be both, refractive index and absorption modulated,[46] in the first case the grating is most efficient at the highest index of refraction, in the second case, the grating is most efficient at maximum absorption. In Figure 4b, the real and imaginary part of the index of refraction of an amorphous dye film as measured by ellipsometry is shown. A strong variation of the refractive index is a natural consequence of the Kramers−Kronig relation at the vicinity of an absorption feature.[47] On the basis of these data, the diffraction behavior of PCBM/CyC gratings was modeled using the FDTD Solutions software. The results of this simulation are shown in Figure 4c. Similarly to the experimental data, the maximum in scattering intensity is not observed at the maximum of absorption, but for the maximum in index of refraction of the dye, notably at 591 nm, suggesting a grating modulated by the index of refraction.

To create periodic line patterns of aggregated dye, a pattern of self-assembled monolayers (SAMs) with 2 μm periodicity was transferred onto a gold substrate by microcontact printing. Blend solutions of PCB−diyne and CyC were spin coated onto the patterned substrates.[48,40] Similarly to the blends coated on homogeneous substrates, the blend laterally phase separates into a CyC phase and a PCB−diyne rich phase. The underlying surface energy pattern directs phase separation, CyC forms continuous stripes on the

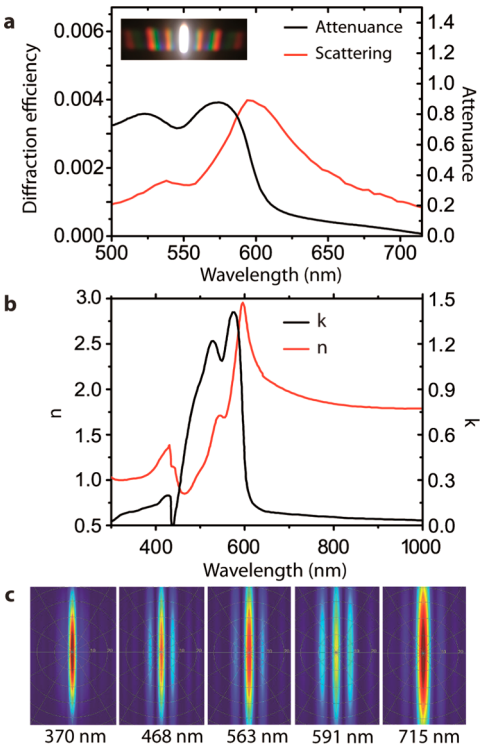

Figure 4. Optical properties of patterned amorphous films. (a) Attenuance and integrated area of the first-order diffracted peak for gratings made of stripes of amorphous dye. Scattering is strongly enhanced for wavelengths with the strongest variation in index of refraction. Inset: dispersion of incident white light into spectral lines. The diffraction efficiency is not wavelength-selective enough to depress scattering away from the peak at 600 nm. (b) Optical constants of a CyC film measured by ellipsometry. (c) Simulation of wavelength-dependent scattering. Scattering is observed throughout the dye absorption, but is strongest at the maximum of n.

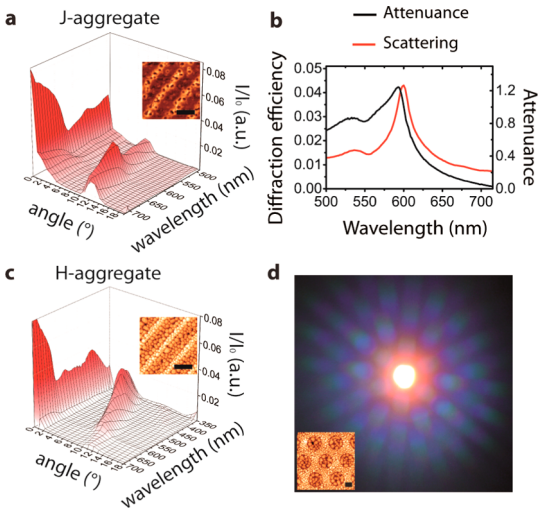

Figure 5. Optical properties of patterned aggregated dye films. (a) Scattering intensity as a function of wavelength and scattering angle for a J-aggregated film. Inset: nanostructured PCB–diyne substrate. (b) Scattering efficiency and attenuance as a function of the wavelength for J-aggregates. (c) Scattering intensity as a function of the wavelength of incoming light and scattering angle for a H-aggregated film. Inset: nanostructured PCBM substrate. (d) Photograph of white light passing through a hexagonally patterned H-aggregate sample (SPM in inset) projected onto a white screen. Only the blue light is scattered. The size of the scale bars is 2.0 μm.

SAM, and a PCB–diyne matrix covered with dye droplets forms on the Au-stripes. The dye can be selectively removed to result in a topographical PCB–diyne grating. An SPM image of the substrate is shown in the inset of Figure 5a. Similar to before, this substrate can be recoated with a saturated dye solution and aggregated dye films form in the voids. Aggregation is again due to the formation of dye droplets pinned to the nanostructured PCB–diyne surface. Figure 5a is a 3D presentation of the scattering intensity of a J-aggregated film as a function of wavelength and scattering angle. A sharp maximum is observed around 610 nm at a diffraction angle of 10°, the angular position of the diffracted peak shifts linearly according to the angle dependence of the Bragg law. Figure 5b shows the attenuance and diffraction efficiency as a function of wavelength. When forced onto a line grating, J-aggregation is not as pronounced as in films on isotropically structured substrates. Still, the aggregate component in the film results in a diffraction efficiency that is much sharper compared to the nonaggregated dye grating (Figure 4). Also here the diffraction maximum of the aggregated film is red-shifted with respect to the attenuance features. Figure 5c shows the same situation for a grating containing H-aggregates formed on a PCBM template.[48] Notable here is the strong wavelength selectivity due to the aggregate and the angle selectivity due to the grating. To illustrate this effect visually, Figure 5d shows a projection of white light passing through a film containing H-aggregates on a hexagonal pattern. The H-aggregate attenuation peak (Supporting Information Figure 6) pretty much only extends over the range of blue light in the visible spectrum (450–495 nm). Correspondingly, light scattered into a hexagonal pattern appears blue to the human eye. A direct application of this property is in transparent displays.[49]

CONCLUSIONS

A new method to organize dye chromophores into aggregates in thin films was introduced. J-aggregates precipitate at the contact line of substrate, dye, and air in evaporating droplets of dye solution during spin coating. We can relate this process to an earlier reported mechanism concerning the fabrication of H-aggregates. The aggregates manufactured this way are sticking out for the prominence of scattering in the absorption band. While this behavior is characteristic for large aggregates in solution, we are not aware of any reports in the literature describing such drastic resonant scattering in thin dye aggregate films. The scattering may be compared to scattering of localized surface plasmon resonances (LSPR), suggesting also

here a coherently oscillating electron cloud. Compared to LSPR, for J-aggregates in thin films even narrower band widths have been reported (fwhm = 13.4 nm).[23] A natural next step is to decrease the line width also for the scattering resonance and to enhance transparency for wavelengths away from the resonance. From here, numerous applications in optics, photonics, and sensing can be envisioned.

MATERIALS AND METHODS

Materials. 1,1′-Diethyl-3,3,3′,3′-tetramethylcarbocyanine perchlorate[50] (CyC) and 10,12-tricosadiynoic acid [6,6]-phenyl-C_{61}-butyl ester (PCB−diyne)[40] were synthesized in our laboratory. For structure formulas of the compounds see Supporting Information Figure 1. [6,6]-Phenyl-C_{61}-butyric acid methyl ester (PCBM) was purchased from Solenne B.V., The Netherlands. Solvents were purchased from Aldrich and used without further purification.

Film Formation. Blend films of PCB−diyne and CyC or PCBM and CyC were spin coated from the common solvent chlorobenzene (CB) onto glass substrates at 1000 rpm. The film thickness was adjusted by varying the solution concentration (from 0.1 to 2.4 wt %). CyC films were spin coated at 1000 rpm from saturated ethanol solutions (10.2 mg/mL) and saturated isopropyl alcohol solutions (1.2 mg/mL) onto different substrates.

Structured Substrates. Nanostructured surfaces were created through phase separation of two immiscible substances during a solvent quench and selectively removing one phase. In the PCBM/CyC blends, CyC could be selectively removed from the blend films by immersing the sample in 2,2,3,3-tetrafluoropropanol (TFP). In the PCB−diyne/CyC blends, PCB−diyne was stabilized at 120 °C for 7 h[40] and dipped in chlorobenzene to selectively remove the dye. Polystyrene (M_w = 560K, Fluka Analytic, Switzerland) and PVME (M_w = 90K, Scientific Polymer Products, Inc., Ontario, NY) were mixed with 0.17 and 0.37 wt %, respectively, in toluene and spin-coated at 3000 rpm on glass. The films were dried under vacuum (10^{-4} bar) overnight and then annealed at 150 °C for 5−30 min. The films were then washed in water for 20 min to remove PVME and dried under nitrogen flow. Patterned self-assembled monolayer (SAMs) substrates were obtained by microcontact printing of octadecanethiol (Sigma-Aldrich) from a poly(dimethylsiloxane) stamp onto gold.[42]

Characterization. Scanning Probe Microscopy (SPM) images were done on a NanoSurf Mobile S (Nanosurf AG, Switzerland) in tapping mode at 170 kHz with rectangular silicon cantilevers (Nanosensors; Mikromasch, Lady's Island, SC), with a force constant of ~40 N m^{-1} and tip radius of 10 nm. The images were analyzed with the WsXM software. The UV−vis spectrophotometer used was a Varian Cary 50. Absorbance spectra were measured on a Horiba Jobin Yvon Fluorolog equipped with an integrating sphere, following the procedure described in ref 44. Light diffraction was measured with a photodiode mounted to a motorized goniometer. The light source is a xenon-lamp (LOT-Oriel, U.K.) coupled to a monochromator (Omni-λ300, Zolix, China). The beam was optically focused on the sample surface. Solvent evaporating times during spin coating were measured by laser reflectometry on glass substrates.[51] Simulations were done with the program FTDT Solutions from Lumerical Solutions, Inc., Canada. Ellipsometry was performed on a spectroscopic Ellipsometer, M-2000U from J.A. Woollam (Lincoln, NE).

Data Processing. For graphical representation in Figure 3b, the raw intensity data I obtained from the diffraction setup was integrated over the scattering ring and normalized by the lamp intensity I_0. For graphical representation in Figures 4 and 5, the raw data was normalized by the lamp intensity. No integration was performed as the diffraction occurs in-plane with the detector. In this case, the diffraction efficiency is defined as the integral of the first-order diffraction peak normalized to the integral of the zeroth-order peak.

Conflict of Interest: The authors declare no competing financial interest.

Acknowledgment. We acknowledge funding from the Swiss National Science Foundation (SNSF) under Grant No. 200020_149127 and under R'Equip no. 206021-121306, Ü. Müller and the Swiss Scanning Probe Microscopy User Laboratory at EMPA for SPM support, Thomas Geiger (EMPA) for dye synthesis, Erwin Hack (EMPA) for support on ellipsometry. We thank Rolf Steiger for helpful discussions.

Supporting Information Available: Structural formulas of chemical compounds, SPM scans of the morphology of both template films and dewetted CyC films, UV−vis spectra showing the removal of H-aggregates in hexane from CyC/PCB−diyne films, the attenuance spectrum of a PCBM/CyC blend film on a hexagonally patterned gold/SAM substrate, fluorescence data of a J-aggregated and a nonaggregated film and a table summarizing the key properties of the solvents used in this study. This material is available free of charge *via* the Internet at http://pubs.acs.org.

REFERENCES AND NOTES

1. Kuhn, H.; Kuhn, C. Chromophore Coupling Effects. In *J-Aggregates*; Kobayashi, T., Ed.; World Scientific: Singapore, 1996; pp 1−40.
2. Wurthner, F.; Kaiser, T. E.; Saha-Möller, C. R. J-Aggregates: From Serendipitous Discovery to Supramolecular Engineering of Functional Dye Materials. *Angew. Chem., Int. Ed.* **2011**, *50*, 3376–3410.
3. Mobius, D. Cooperative Phenomena in Organized Monolayers. *Z. Phys. Chem., Neue Folge* **1987**, *154*, 121–144.
4. Scheibe, G. Auxiliary Valency as the Cause of Variability in the Absorption Spectra in Solutions. *Angew. Chem.* **1937**, *50*, 0212–0219.
5. Jelley, E. E. Spectral Absorption and Fluorescence of Dyes in the Molecular State. *Nature* **1936**, *138*, 1009–1010.
6. Emerson, E. S.; Conlin, M. A.; Rosenoff, A. E.; Norland, K. S.; Rodrigue, H.; Chin, D.; Bird, G. R. Geometrical Structure and Absorption Spectrum of a Cyanine Dye Aggregate. *J. Phys. Chem.* **1967**, *71*, 2396–2403.
7. Jones, R. M.; Lu, L. D.; Helgeson, R.; Bergstedt, T. S.; McBranch, D. W.; Whitten, D. G. Building Highly Sensitive Dye Assemblies for Biosensing from Molecular Building Blocks. *Proc. Natl. Acad. Sci. U.S.A.* **2001**, *98*, 14769–14772.
8. Gadonas, R. Nonlinear Optical Properties of Pseudoisocyanine. In *J-Aggregates*; Kobayashi, T., Ed.; World Scientific: Singapore, 1996; pp 181−198.
9. Naber, A.; Fischer, U. C.; Kirchner, S.; Dziomba, T.; Kollar, G.; Chi, L. F.; Fuchs, H. Architecture and Surface Properties of Monomolecular Films of a Cyanine Dye and their Light-Induced Modification. *J. Phys. Chem. B* **1999**, *103*, 2709–2717.
10. Hranisavljevic, J.; Dimitrijevic, N. M.; Wurtz, G. A.; Wiederrecht, G. P. Photoinduced Charge Separation Reactions of J-Aggregates Coated on Silver Nanoparticles. *J. Am. Chem. Soc.* **2002**, *124*, 4536–4537.
11. Tischler, J. R.; Bradley, M. S.; Bulovic, V.; Song, J. H.; Nurmikko, A. Strong Coupling in a Microcavity LED. *Phys. Rev. Lett.* **2005**, *95*, 036401.
12. Kozhekin, A. E.; Kurizki, G.; Malomed, B. Standing and Moving Gap Solitons in Resonantly Absorbing Gratings. *Phys. Rev. Lett.* **1998**, *81*, 3647–3650.
13. Pasternack, R. F.; Collings, P. J. Resonance Light Scattering: A New Technique for Studying Chromophore Aggregation. *Science* **1995**, *269*, 935–939.
14. Anglister, J.; Steinberg, I. Z. Resonance Rayleigh Scattering of Cyanine Dyes in Solution. *J. Chem. Phys.* **1983**, *78*, 5358–5368.

15. Lu, W.; Band, B. S. F.; Yu, Y.; Li, Q. G.; Shang, J. C.; Wang, C.; Fang, Y.; Tian, R.; Zhou, L. P.; Sun, L. L.; *et al.* Resonance Light Scattering and Derived Techniques in Analytical Chemistry: Past, Present, and Future. *Microchim. Acta* **2007**, *158*, 29–58.
16. Hutter, E.; Fendler, J. H. Exploitation of Localized Surface Plasmon Resonance. *Adv. Mater.* **2004**, *16*, 1685–1706.
17. Garcia, M. A. Surface Plasmons in Metallic Nanoparticles: Fundamentals and Applications. *J. Phys. D: Appl. Phys.* **2011**, *44*, 283001.
18. Tani, T. *Photographic Science*; Oxford University Press: Oxford, U.K., 2011.
19. Editorial: Organics Settle Down. *Nat. Nanotechnol.* **2009**, *4*, 607.
20. Lehmann, U. Aggregation of Cyanine Dyes at Langmuir-Blodgett Monolayers. *Thin Solid Films* **1988**, *160*, 257–269.
21. Fukumoto, H.; Yonezawa, Y. Layer-by-Layer Self-Assembly of Polyelectrolyte and Water Soluble Cyanine Dye. *Thin Solid Films* **1998**, *329*, 748–751.
22. Dahne, L. Self-Organization of Polymethine Dyes in Thin Solid Layers. *J. Am. Chem. Soc.* **1995**, *117*, 12855–12860.
23. Steiger, R.; Pugin, R.; Heier, J. J-Aggregation of Cyanine Dyes by Self-Assembly. *Colloids Surf., B* **2009**, *74*, 484–491.
24. Misawa, K.; Ono, H.; Minoshima, K.; Kobayashi, T. New Fabrication Method for Highly Oriented J-Aggregates Dispersed in Polymer Films. *Appl. Phys. Lett.* **1993**, *63*, 577–579.
25. Peyratout, C. S.; Mohwald, H.; Dahne, L. Preparation of Photosensitive Dye Aggregates and Fluorescent Nanocrystals in Microreaction Containers. *Adv. Mater.* **2003**, *15*, 1722–1726.
26. Heier, J.; Groenewold, J.; Huber, S.; Nuesch, F.; Hany, R. Nanoscale Structuring of Semiconducting Molecular Blend Films in the Presence of Mobile Counterions. *Langmuir* **2008**, *24*, 7316–7322.
27. Nuesch, F.; Moser, J. E.; Shklover, V.; Gratzel, M. Merocyanine Aggregation in Mesoporous Networks. *J. Am. Chem. Soc.* **1996**, *118*, 5420–5431.
28. Heier, J.; Steiger, R.; Nuesch, F.; Hany, R. Fast Assembly of Cyanine Dyes into Aggregates onto [6,6]-Phenyl C_{61}-Butyric Acid Methyl Ester Surfaces from Organic Solvents. *Langmuir* **2010**, *26*, 3955–3961.
29. Stannard, A. Dewetting-Mediated Pattern Formation in Nanoparticle Assemblies. *J. Phys.: Condens. Matter* **2011**, *23*, 083001.
30. Hu, H.; Larson, R. G. Evaporation of a Sessile Droplet on a Substrate. *J. Phys. Chem. B* **2002**, *106*, 1334–1344.
31. Deegan, R. D.; Bakajin, O.; Dupont, T. F.; Huber, G.; Nagel, S. R.; Witten, T. A. Capillary Flow As the Cause of Ring Stains from Dried Liquid Drops. *Nature* **1997**, *389*, 827–829.
32. Bhardwaj, R.; Fang, X. H.; Attinger, D. Pattern Formation During the Evaporation of a Colloidal Nanoliter Drop: a Numerical and Experimental Study. *New J. Phys.* **2009**, *11*, 075020.
33. Govor, L. V.; Reiter, G.; Parisi, J.; Bauer, G. H. Self-Assembled Nanoparticle Deposits Formed at the Contact Line of Evaporating Micrometer-Size Droplets. *Phys. Rev. E* **2004**, *69*, 061609.
34. Li, H. Y.; Tee, B. C. K.; Cha, J. J.; Cui, Y.; Chung, J. W.; Lee, S. Y.; Bao, Z. N. High-Mobility Field-Effect Transistors from Large-Area Solution-Grown Aligned C_{60} Single Crystals. *J. Am. Chem. Soc.* **2012**, *134*, 2760–2765.
35. Tisserant, J. N.; Wicht, G.; Gobel, O. F.; Bocek, E.; Bona, G. L.; Geiger, T.; Hany, R.; Mezzenga, R.; Partel, S.; Schmid, P.; *et al.* Growth and Alignment of Thin Film Organic Single Crystals from Dewetting Patterns. *ACS Nano* **2013**, *7*, 5506–5513.
36. Hashimoto, Y.; Karthaus, O. Preparation of an Ordered Array of Cyanine Complex Microdomes by a Simple Dewetting Method. *J. Colloid Interface Sci.* **2007**, *311*, 289–295.
37. Gentili, D.; Foschi, G.; Valle, F.; Cavallini, M.; Biscarini, F. Applications of Dewetting in Micro and Nanotechnology. *Chem. Soc. Rev.* **2012**, *41*, 4430–4443.
38. Kargupta, K.; Konnur, R.; Sharma, A. Instability and Pattern Formation in Thin Liquid Films on Chemically Heterogeneous Substrates. *Langmuir* **2000**, *16*, 10243–10253.
39. Seemann, R.; Brinkmann, M.; Kramer, E. J.; Lange, F. F.; Lipowsky, R. Wetting Morphologies at Microstructured Surfaces. *Proc. Natl. Acad. Sci. U.S.A.* **2005**, *102*, 1848–1852.
40. Tisserant, J. N.; Hany, R.; Wimmer, E.; Sanchez-Ferrer, A.; Adamcik, J.; Wicht, G.; Nuesch, F.; Rentsch, D.; Borgschulte, A.; Mezzenga, R.; *et al.* Diyne-Functionalized Fullerene Self-Assembly for Thin Film Solid-State Polymerization. *Macromolecules* **2014**, *47*, 721–728.
41. Ogawa, H.; Kanaya, T.; Nishida, K.; Matsuba, G. Phase Separation and Dewetting in Polystyrene/Poly(vinyl methyl ether) Blend Thin Films in a Wide Thickness Range. *Polymer* **2008**, *49*, 254–262.
42. Kumar, A.; Whitesides, G. M. Features of Gold Having Micrometer to Centimeter Dimensions Can Be Formed Through a Combination of Stamping with an Elastomeric Stamp and an Alkanethiol "Ink" Followed by Chemical Etching. *Appl. Phys. Lett.* **1993**, *63*, 2002–2004.
43. Heier, J.; Steiger, R.; Hany, R.; Nuesch, F. Template Synthesis of Cyanine Dye H-Aggregates on Nanostructured [6,6]-Phenyl C_{61}-Butyric Acid Methyl Ester Substrates. *Phys. Chem. Chem. Phys.* **2011**, *13*, 15714–15722.
44. DeMello, J. C.; Wittmann, H. F.; Friend, R. H. An Improved Experimental Determination of External Photoluminescence Quantum Efficiency. *Adv. Mater.* **1997**, *9*, 230–232.
45. Zhao, X. M.; Stoddart, A.; Smith, S. P.; Kim, E.; Xia, Y. N.; Prentiss, M.; Whitesides, G. M. Fabrication of Single-Mode Polymeric Waveguides Using Micromolding in Capillaries. *Adv. Mater.* **1996**, *8*, 420–424.
46. Magnusson, R.; Gaylord, T. K. Diffraction Regimes of Transmission Gratings. *J. Opt. Soc. Am.* **1978**, *68*, 809–814.
47. Prineas, J. P.; Zhou, J. Y.; Kuhl, J.; Gibbs, H. M.; Khitrova, G.; Koch, S. W.; Knorr, A. Ultrafast AC Stark Effect Switching of the Active Photonic Band Gap from Bragg-Periodic Semiconductor Quantum Wells. *Appl. Phys. Lett.* **2002**, *81*, 4332–4334.
48. Tisserant, J. N.; Hany, R.; Partel, S.; Bona, G. L.; Mezzenga, R.; Heier, J. Dewetting-Driven Hierarchical Self-Assembly of Small Semiconducting Molecules. *Soft Matter* **2012**, *8*, 5804–5810.
49. Hsu, C. W.; Zhen, B.; Qiu, W. J.; Shapira, O.; DeLacy, B. G.; Joannopoulos, J. D.; Soljacic, M. Transparent Displays Enabled by Resonant Nanoparticle Scattering. *Nat. Commun.* **2014**, *5*, 3152.
50. Ernst, L. A.; Gupta, R. K.; Mujumdar, R. B.; Waggoner, A. S. Cyanine Dye Labeling Reagents for Sulfhydryl Groups. *Cytometry* **1989**, *10*, 3–10.
51. Jukes, P. C.; Heriot, S. Y.; Sharp, J. S.; Jones, R. A. L. Time-Resolved Light Scattering Studies of Phase Separation in Thin Film Semiconducting Polymer Blends during Spin-Coating. *Macromolecules* **2005**, *38*, 2030–2032.